2024 IEEE/RSJ International Conference on Intelligent Robots and Systems (IROS)
October 14-18, 2024. Abu Dhabi, UAE

A Tetherless Soft Robotic Wearable Haptic Human Machine Interface for Robot Teleoperation

Shilpa Thakur*, Nathalia Diaz Armas+, Joseph Adegite*, Ritwik Pandey*, Joey Mead+, Pratap M. Rao*, Cagdas D. Onal*

***Abstract*— This work describes the development, demonstration, and performance evaluation study of a wearable human machine interface for robotic teleoperation. We present a novel tetherless human machine interface in the form of a backpack, wearable 3D arm motion capture sensors, finger flexion sensors, and pneumatic haptic feedback muscles. The system is integrated in a complete teleoperation framework, enabling users to be immersed in a remote environment through virtual reality headgear, facilitating intuitive manipulation of an industrial articulated arm. The human machine interface samples the kinematic configuration of the user's arm, hand, and fingers using multiple inertial measurement units and capacitive sensors respectively, and streams it to the teleoperation software stack. The gripping forces experienced at the robot's end-effector are acquired using a custom three-dimensional Hall-effect magnetic sensor. The system simultaneously renders the kinesthetic and tactile feedback on the user's fingers through custom designed pneumatically actuated soft robotic haptic muscles. The efficacy of the human machine interface and the teleoperation system was tested and evaluated by conducting user studies, which showed 31.4% faster teleoperation compared to a keypad controller, and 60% less gripping force utilized with haptics enabled. The findings of the study guided the design and prototype development of a printed electronics based stretchable sleeve and glove motion capture unit to improve the portability, ergonomics, and user experience of the human machine interface.**

I. Introduction

Teleoperation systems are deeply integrated into various fields, including remote surgeries, telenursing, space exploration, underwater missions, mining, and agriculture [1-4]. Such systems enable users to execute tasks that are perilous and require human intervention from a distant location. Teleoperation systems can also be used for training the remotely deployed robots in unstructured environments to learn new complex tasks from an expert human demonstrator. When faced with dynamic environments, teleoperation systems are favored over autonomous systems due to the human operator's superior learning ability and adaptability. Teleoperation can be more intuitive and lifelike when the system emulates the response and perceived kinesthetic characteristics of a human arm that has been extended into the remote environment. The application of teleoperation is currently restricted by the presence of large, immobile teleoperation systems [5]. Thus, portability and seamless control are crucial for Human Robot Interaction (HRI).

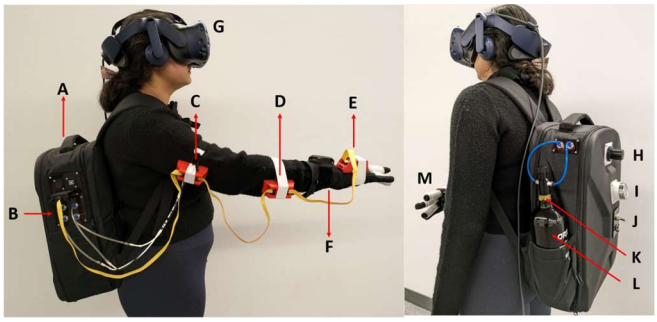

Figure 1. HMI hardware components: backpack unit (A), system I/O panel (B), upper arm IMU (C), forearm IMU (D), wrist IMU (E), Stretch Sense finger motion capture glove (F), VR headgear (G), pneumatic pressure regulator knob (H), pressure gauge (I), power switch and external DC power input (J), air tank pressure relief valve (K), air tank (L), haptic muscles (M).

In addition to visual feedback, haptic feedback is important to realize an intuitive teleoperation experience, fine motor control, and ability to manipulate fragile objects [6]. These haptic devices function as interactive interfaces for users in virtual environments in a wearable form factor [7][8]. They capture the finger position, hand position, orientation, and button click which can be assigned various functions. These devices render static forces, dynamic forces, vibrations, pressure, texture, and heat for haptic feedback [9-11].

This paper describes the development and demonstration of an all-in-one wearable HMI in the form of a glove, sleeve, and a backpack which houses the control and power systems. The device features an inertial measurement unit (IMU) based motion capture of the human arm and provides haptic feedback to the user. In this study, we have showcased the teleoperation of the Kinova Gen 3 robotic arm, equipped with a Robotiq 2F-85 gripper as its end-effector using our HMI. The entire wearable pneumatic based haptic feedback system is built around specially designed pneumatic soft actuators, which we call "haptic muscles". The fabrication process is similar to Pneumatic Artificial Muscle (PAM), however haptic muscles are designed for constrained lateral expansion than axial. Haptic muscles are worn around the user's fingers, which simulate the grasp force experienced at the robot's end effector on controlled pressurization.

The research in this work is supported by SEMI-FlexTech under Grant no. FT19-21-215, the Massachusetts Manufacturing Innovation Initiative (M2I2), National Science Foundation (NSF) under Grant Nos. DGE-1922761 and IIS-2024802, Amazon's Greater Boston Tech Initiative Award (GBTI).

*Worcester Polytechnic Institute (WPI), Worcester MA 01609, USA Shilpa Thakur, Ritwik Pandey and Cagdas D. Onal (Corresponding Author) are with the Robotics Engineering Department. Joseph Adegite and Pratap M. Rao are with the Mechanical and Materials Engineering Department {sthakur, rpandey, joadegite, pmrao, cdonal}@wpi.edu

+ University of Massachusetts Lowell (UMass Lowell, Lowell MA 01854, USA. Nathalia Dias Armas (Nathalia_DiazArmas@student.uml.edu) and Joey Mead (Joey_Mead@uml.edu) are with the Plastics Engineering Department.

In our group's previous work, we fabricated a fabric-silicone composite based pneumatic bladder to render haptic feedback during teleoperation [11]. However, the manufacturing process was not streamlined or easily adjusted. In this paper, we created a woven fiber reinforced haptic muscle that is covered with an elastomeric material. Such a structure, where the yarns are interlaced diagonally about an axis, in conjunction with an impregnated elastomeric matrix, imparts superior mechanical properties compared to their individual components, while also providing design flexibility [12][13]. To measure the gripping force at the robot's end-effector, we integrated a custom Hall-effect based three-dimensional force sensor. The sensor's basic working principle and a prototype using a silicone molded compliant structure was developed and its performance was validated by our group in a previous work [12][13]. Using this experience, we developed and integrated a gripper force sensor specific to our requirements as explained below. Lastly, a wearable sleeve and glove HMI device was developed based on printed electronics to improve the form factor and user experience.

II. Wearable Haptic Human Machine Interface

A. System Overview and Architecture

The wearable HMI as shown in Fig. 1 consists of the backpack (A), three custom designed arm-strapped IMU modules (C, D, E), capacitive sensor-based hand motion capture glove (F), and pneumatically actuated soft haptic muscles (M). The Virtual Reality (VR) headgear (G) isolates the user's visual and auditory senses from their physical surroundings and feeds them with the video streamed from a tele-operated robot's camera as described later in detail.

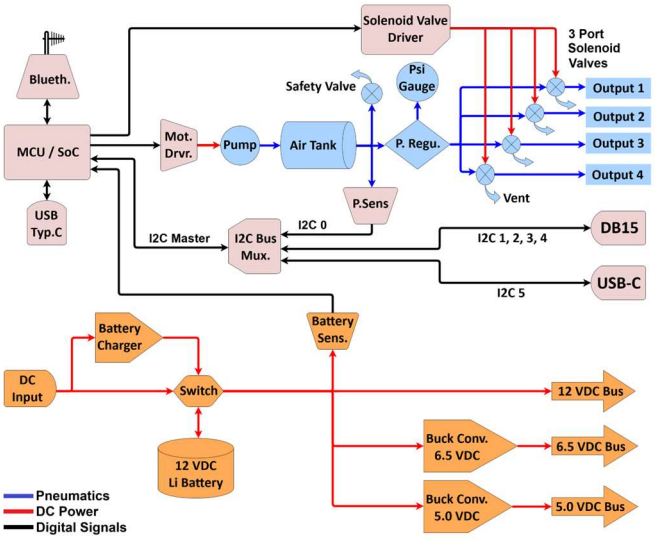

Figure 2. Backpack System Overview.

The backpack houses the critical hardware and controls as shown in Fig. 2 which are responsible for motion capture and rendering haptic feedback to the user. It offers Bluetooth and USB interfaces to the desktop computer that hosts the teleoperation software stack implemented on Robot Operating System (ROS) Noetic Ninjemys distribution. The system is powered by a 12 V Li-ion Battery or with a 12 VDC input delivered by an AC to DC adapter via a DC power input connector provided on the power panel also used for charging the on-board battery (labeled J in Fig. 1). The battery management system (BMS) consists of over-voltage, under-voltage, over-current, and under-current protection. It allows the backpack to operate on external DC input, while simultaneously charging the battery if it is below a threshold voltage. The battery voltage is also reported to the microcontroller in the form of an analog signal scaled to a maximum of 5 VDC for a battery voltage of 12 VDC. Digital buck converters generate 6.5 VDC and 5 VDC by regulating the 12 VDC battery voltage for powering specific components like the Texas Instruments L293D integrated circuit (IC) pneumatic solenoid valve driver, a Microchip ATmega 2560 microcontroller unit (MCU), a Texas Instruments TCA9548A inter-integrated circuit (I^2C) serial multiplexer, an I^2C serial interfaced Adafruit MPRLS ported pressure sensor rated to a max pressure of 25 psi and the arm strapped motion capture hardware.

An air compressor pump rated at 12 VDC, 24 Watts is driven by the BTS7960 high power half H-bridge motor driver that derives power directly from the BMS. The pump has a free flow rate of 8.8 L/min at up to 12 psi of pressure. The compressed air from the pump is stored in a lightweight aluminum air accumulator (labelled L in Fig. 1) with the maximum limit of 3000 psi. The safety pressure relief valve (K) releases excess pressure in case the accumulator reaches its storage limit. The MPRLS pressure sensor is used by the MCU to monitor the accumulator pressure and trigger the air compressor to recharge the accumulator according to a pressure threshold window. The threshold window consists of two thresholds, 10 and 13 psi. When the sensed pressure drops below 10 psi, the compressor is activated till the pressure exceeds the higher threshold. At 13 psi, the compressor is turned off until the pressure drops below the lower threshold. This dead-zone bang-bang pressure control approach conserves the system battery by avoiding frequent pumping cycles during teleoperation. A pressure regulator (labelled H) is employed to provide air supply at a constant set pressure to the SMC Pneumatics S070C-VAG-32 three-port solenoid valves, which actuate the pneumatic haptic muscles. The pressure dial (I) allows the user to adjust the output of the pressure regulator such that it does not exceed the maximum operating limit of the haptic muscles, tested to be 7 psi.

The spatial orientation and position (pose) of the user's arm is captured using three arm-strapped IMU modules employing the Bosch BNO055 IC interfaced by I^2C serial protocol. Since the IMUs can only be assigned two possible addresses, connecting all the three via a single I^2C bus to the microcontroller is not possible, as it would result in address conflicts. Therefore, each of them is interfaced with the TCA9548A I^2C serial multiplexer, which can selectively stream data via a single channel interfaced with the system's microcontroller. This implementation required dedicated clock and data lines along with a shared pair of power lines, thus 8 connection lines in total. The connections from the IMU are delivered to the backpack at the I/O panel (labeled B in Fig. 1), which has a 15 pin D-Sub female connector, with 7 pins provided for expandability.

The user's finger motion is captured using the Stretch Sense SuperSplay glove interfaced with the PC via Bluetooth. The glove senses the degree by which the user bends their

finger using soft capacitors stitched into the glove's fabric along each finger [14]. The soft capacitor's basic construction includes a stretchable electrode sandwiched between two silicone dielectric insulators, which are sandwiched between two reference electrodes connected to ground potential. The soft capacitive sensor exhibits a change in capacitance when it is physically stretched or relaxed along the electrode's plane or normal. The change in capacitance is detected, filtered and quantified by mixed-signal circuits [15][16].

B. Manufacturing and Testing of Haptic Muscles

The pneumatically actuated soft robotic haptic muscles were designed in such a way that they would be easy to wear, lightweight (up to 25 g), exhibit a fast dynamic response and deviation in steady-state linearity under 5%. The haptic muscles exert two components of forces on the human finger, restoration and compression. As the muscles are pressurized, they gently restore the user's fingers replicating the kinesthetic sensation akin to the grasp force felt by a robotic gripper. Simultaneously, the compression force creates a sensation of finger squeezing, offering tactile feedback to the user.

In this study, we fabricated the DOWSIL 92-009 silicone haptic muscle reinforced with nylon fibers and compared its performance with the cotton-spandex and Eco Flex 0030 based variant of haptic muscle that our team had developed in previous work [11]. The manufacturing process for the DOWSIL 92-009 silicone haptic muscle, involved four sequential stages, Fig. 3. The first stage involved fabricating a tubular braided nylon fiber reinforcement shell using a braiding machine. The purpose of customizing the braiding is to experiment with various braiding pitch and yarn materials. However, elaboration of these studies is out of the scope of this article.

The braiding machine featured 16 rotating braiding yarn spools. We used SgtKnots size #69 bonded nylon thread as the braiding fiber material. The machine braids the Nylon yarn around two different PTFE (polytetrafluoroethylene) cores with a diameter of 25.4 and 22.2 mm, rendering two distinct tubular structures of inner diameter which was the same as the PTFE cores. The PTFE cores provided a non-stick surface for the easy removal of the composite material once completely fabricated. The second stage of fabrication began by mounting the nylon braided Teflon cores on a motor driven rotary chuck. The braided nylon was impregnated with DOWSIL 92-009 dispersion coating clear silicone elastomeric matrix manufactured by Dow Inc. using a multi-layer coating process. The coating process involved four consecutive coating and drying routines with a drying period of 30 minutes, while rotating the Teflon cores at constant speed of 30 RPM. The rotating composite tubular mass was left for 72 hours to complete the cure. Prior to coating, the silicone was thinned using a mixture of Varnish Maker and Painters Naphtha produced by Klean Strip, in a volume ratio of 4 parts thinner to 3 parts silicone. The third stage entailed removing the elastomeric composite tubes from the Teflon cores and trimming them to the desired lengths. The composite tube with an inner diameter of 22.2 mm was cut about 10 mm longer than the 25.4 mm tube. The composite tubes were then coaxially stacked and a polyurethane (PU) air tube of 3.5 mm was inserted to a length of 10 mm into the space between the two composite tubes. In the fourth and final stage, the stacked composite tubes were placed on a Teflon core and mounted on the rotary chuck. The open ends of the tube stack were coated with undiluted silicone, while the chuck spun at 30 RPM. This final silicone coating was used to seal the gap between composites and the air tube connection. After curing, the assembled Nylon fiber reinforced Silicone haptic muscle was extracted from the Teflon rod. The fiber reinforced elastomeric composite material offers enhanced mechanical strength, durability, impermeability and tunability of mechanical characteristics such as rigidity and elasticity.

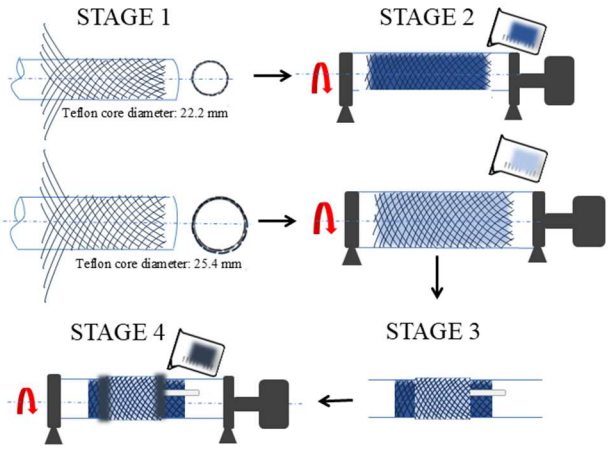

Figure 3. Haptic Muscle Manufacturing process.

The haptic muscle was characterized for its restoration, compression force and time domain response on a custom designed jig (supplementary video) [11]. The jig consists of a 3D printed tendon-driven anthropomorphic finger linked to a load-cell to measure the restoration force. A force sensing resistor (FSR) was mounted on the middle phalange of the finger to measure the experienced compression force. The load-cell and the FSR were calibrated to an accuracy of 0.1 g before being mounted on the jig. The setup includes a digital I^2C interfaced MPRLS pressure sensor to measure the haptic muscle pressure. The muscle pressure is controlled by an SMC Pneumatics S070C-VAG-32 three-port solenoid valve driven by pulse width modulation (PWM) of its 6 VDC coil voltage using an L293D solenoid driver IC. The duty cycle of the PWM coil voltage proportionally controls the steady-state pressure of the haptic muscle between a dead zone as seen in Fig. 4. This control scheme is employed in the HMI backpack for rendering the haptic feedback on the user's fingers.

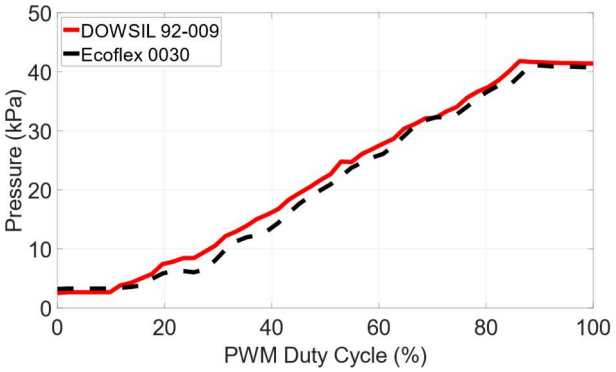

Figure 4. Pressure transfer characteristics of the EcoFlex and the DOWSIL pneumatic haptic muscles, relative to the duty cycle of the PWM coil voltage input to the solenoid valve.

The pressurization characteristics exhibit linear proportionality to the PWM input with a standard deviation of 7 kPa beyond a dead-zone of 10 % duty cycle for the DOWSIL muscle and 15 % for the EcoFlex muscle as seen in Fig. 4. This dead-zone exists because the solenoid valve's spring requires a threshold force to move the plunger off the orifice. The plunger's force opposing the spring is the sum of the forces exerted by the solenoid and the air pressure at the orifice. A shorter dead-zone in pressurization of the DOWSIL muscle is observed as its internal air pressure rises slightly faster than the EcoFlex muscle. This is because of DOWSIL muscle's higher stiffness, attributed to its fiber reinforcement. Both the muscle's internal pressure rises linearly up to 85 % beyond which it saturates as the valve's solenoid is energized enough to completely displace the plunger off the orifice. These tests showed that it was feasible to render linearly varying haptic feedback using the soft robotic haptic muscles. Next, the physical forces rendered by the haptic muscles were characterized.

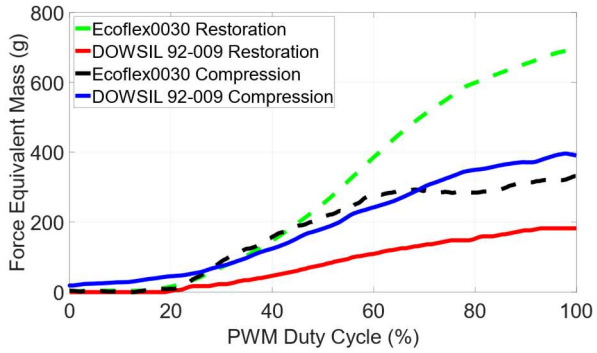

Figure 5. Restoration and compression force transfer characteristics.

It is inferable from the graph shown in Fig. 5 that the haptic muscles are nonlinear in their elastic characteristics. In the case of the DOWSIL muscle, compression force dominates the restoration force exerted on the human finger. This is because the nylon fiber reinforcement causes the muscle to exhibit a higher coefficient of expansion normal to the inner cylindrical surfaces than along the longitudinal and hoop axes. However, the restoration force dominates the compression force in the case of the EcoFlex muscle. This is because it is made using cotton-spandex fabric reinforcement, which is more elastic than nylon fiber braiding. Thus, the EcoFlex muscle exhibits a higher ratio between the coefficient of expansion along the hoop and longitudinal directions of its cylindrical surfaces, in the interior and exterior. Thus, the EcoFlex muscle exerts a higher restoration force up to 700 g as compared to DOWSIL muscle, which plateaus at 200 g at 100% duty cycle.

The maximum compression force experienced by a user for the DOWSIL muscle is equivalent to 400 g, and 330 g for EcoFlex muscle, which are safe for human fingers. The compression force would feel uncomfortable and be safety critical only beyond 17 N or equivalent to 1.73 Kg [17]. The user begins perceiving a compression force only beyond 5 % duty cycle in the case of the DOWSIL muscle and 15 % in the case of the EcoFlex muscle. The restoration force is experienced beyond 20 % duty cycle for both of the muscles. It varies linearly up to 80 % for the EcoFlex muscle and only up to 60 % in the case of the DOWSIL muscle, beyond which it plateaus. From this experiment it was inferred that the EcoFlex muscle has a wider linear range of rendering restoration force compared to the DOWSIL muscle. The restoration force should exceed the compression force as it is crucial for the user's fingers to noticeably straighten in order to realistically perceive the grasp force. Therefore, the EcoFlex muscle was used for haptic rendering in the wearable HMI.

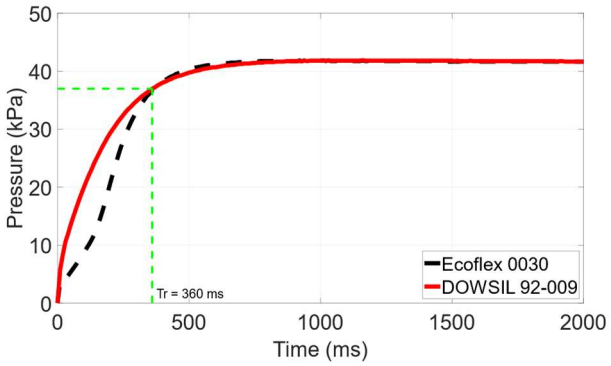

Figure 6. Step response curve of the two versions of haptic muscle.

In order to characterize the dynamic step response of the haptic muscle seen in Fig. 6, we instantaneously inflated the muscle at 100% duty cycle and sampled the muscle pressure for 2 seconds at 100 samples per second. The rise time (t_R) of both the muscles was found to be 360 ms and the slew rate of the overall controller-actuator system to be 0.1 kPa/ms. This shows that the haptic feedback rendering response within a window of 61 ms, beyond which the user can discriminate delays [18], is 6.1 kPa. Thus, the control system and the driven actuator are characteristically quick enough to be barely noticeable of its transitions between various PWM control inputs.

C. Development of Hall Effect Magnetic Force Sensor

In order to sense the grasp force experienced at the robot's gripper, we developed a three-dimensional force sensor by employing a linear 3D Hall-effect magnetic field sensor and a miniature magnet mounted on a custom designed compliant mechanism, 3D printed using soft polylactic acid (PLA) material. The compliant mechanism design encloses the magnetic field sensor as shown in Fig. 7(B and C). The neck like projection of the compliant structure holds a cylindrical NeFeB magnet seen on the left side of Fig. 7(A).

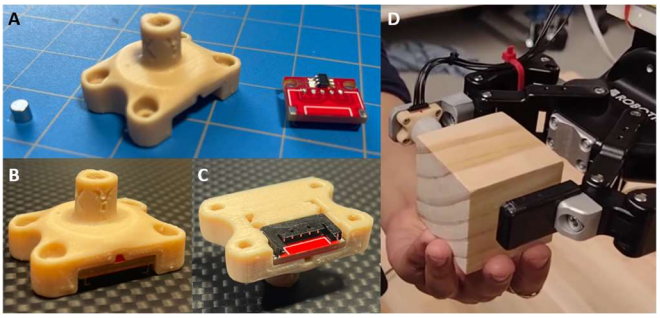

Figure 7. Linear 3D Hall-effect gripper force sensor: Components (A), assembled sensor's top view (B), bottom view (C), and installation (D).

A custom printed circuit board (PCB) containing the Texas Instruments TMAG5273 3D Hall-effect magnetic field I^2C interfaced sensor chip and a 4-pin connector is installed below the sensor body. The body is designed such that the neck of the

sensor is compliant enough to move the magnet along three dimensions (X, Y, Z) relative to the sensor chip. The spatial position of the magnet determines the three-dimensional proximity to the sensor chip which resolves its magnetic field intensity along the X, Y, Z directions. The stiffness of the compliant structure determines the range of linear displacement proportional to applied force, within the sensing range of the magnetic sensor. The sensor was mounted on a custom designed 3D printed finger for Robotiq 2F-85 gripper as shown in Fig. 7(D). In the current application of this sensor, forces along the Z axis are considered and calibrated. Resolving 3D gripping forces has been set as a future goal.

To calibrate and characterize the sensor, we mounted a calibrated load cell with a maximum capacity of 1 kg at the opposing finger of the gripper. We preferred performing the calibration on the gripper itself instead of designing a dedicated jig as it allowed us to validate its efficacy in serving as a gripper force sensor directly. The gripper was actuated at discrete steps of 0.1 mm, which pressed the custom designed magnetic Hall-effect force sensor against the load-cell. To calibrate, a simple linear map was sufficient, whereby the scale of the magnetic sensor reading was adjusted by multiplying it with a scaling factor and the zero offset error was subtracted. This resulted in a closely tracking force reading from the magnetic sensor relative to the load cell as shown in Fig. 8. The noise observed in the magnetic sensor reading is due to its high sensitivity as the magnet is placed at a close proximity to the chip. The magnetic force sensor sampled at 100 Hz reads linearly up to 1 Kg equivalent of force within a compression of 3 mm in the Z axis, beyond which it saturates.

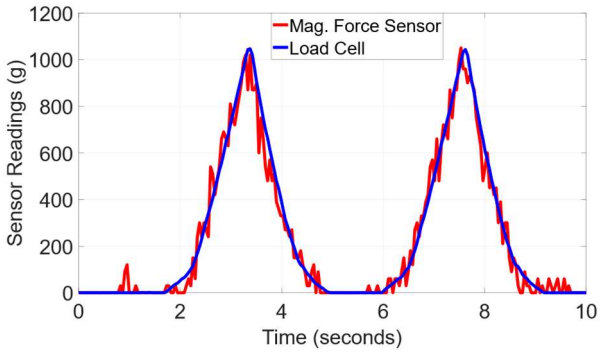

Figure 8. Calibrated magnetic sensor readings and load cell output.

III. Robotic Teleoperation System

In this work, we used a Kinova Gen 3 seven degree of freedom (DOF) articulated robotic arm for telemanipulation using our wearable haptic HMI system. The teleoperation system uses ROS as its backbone for software integration of different sub-systems performing specific functions in the form of nodes. ROS facilitates data exchange between the nodes using custom topics which are data structures containing various messages that represents the data. The software architecture is shown in Fig. 10.

The arm strapped IMU modules placed on the user's upper arm, forearm, and hand of the user provide the arm's joint angles in quaternions. The data is considered as the joint space inputs for the calculation of forward kinematics to determine the position and orientation of the human hand relative to the body frame of the user. The forward kinematic calculation involves a sequence of transformations from the sternum to the shoulder, shoulder to elbow, elbow to wrist and finally wrist to the palm of the user. The workspace of the human is mapped to the robot's workspace by using a simple scaling in Cartesian space. The scaling factor is multiplied to the user's calculated position during teleoperation to calculate the desired position of the robot end effector. This position is passed to the inverse kinematics solver that provides the desired joint angles which are then converted to joint velocities using a simple PID controller. The end-effector poses are also given as an input to the Gazebo simulation environment to virtually simulate the motion of the Kinova Gen 3 following the position and orientation of the human hand represented in a Cartesian frame.

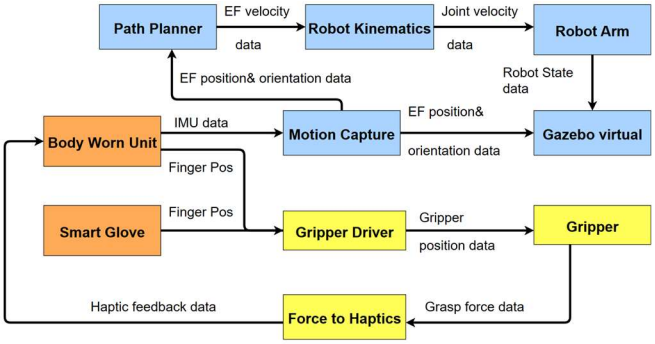

Figure 9. Tele-operation system software block diagram.

The human finger flexion is captured by the Stretch Sense SuperSplay smart glove. The glove transmits 16 bytes of serial data and the finger position corresponds to the first, fifth, eighth, eleventh and fourteenth byte starting from zero. The raw data from the glove is filtered using a low pass filter and then the average of the processed data is linearly mapped to the gripper finger position, which ranges from 0 when completely open and 1 when closed. We implemented an open-loop gripper control to avoid the lags observed in closed-loop control due to the latency in data exchange between various software and hardware abstraction layers. The linear magnetic Hall-effect sensor measures the grasping force at the robot's end-effector. These force readings are relayed to the HMI via USB, which issues linearly mapped PWM values ranging from 0 to 255 to control the solenoid valves that actuate the haptic muscles on the user's finger to provide haptic feedback based on the intensity of the grasping force during teleoperation.

IV. Teleoperation User Studies and Results

In order to study the performance and efficacy of the teleoperation system, we conducted end-user tests approved by our institution's review board under protocol IRB-19-0122. The study included 9 volunteers of ages ranging from 20 to 30 years (6 males, 3 females). The users were visually isolated from their physical environment using the VR headgear which displayed the video feed of the robot's environment via a single Logitech C920x 1080p camera mounted on a tripod (A). The experiment required the users, labelled (B) in Fig. 10, to perform a simple pick-and-place task using the teleoperation system by utilizing the wearable HMI and the keypad controller. The users were made to listen to a pleasant song of their liking via the VR headgear's earphones so that any auditory cues from their physical environment are masked. We

placed three soft toys, which were the target objects of different sizes and forms at random orientations on the left side of the table (D). These were positioned at a fixed distance within the reach of the robot (C) throughout the trials. The users were instructed to place the target objects into a plastic bin (E) fixed on the right. The individual experiments were video graphed and the robot's gripping forces were logged.

The user study included a training phase and a testing phase. During the training phase, each volunteer user was given a briefing about the teleoperation system, the robot control key mappings of the keypad controller, the robot control functionalities and wearing procedure of the HMI system. This briefing was followed by a system demonstration given by the experimenter (i.e. the author), then two assisted user practice runs, and finally two un-assisted practice runs. The users were encouraged to perform practice runs with and without wearing the VR headset to help them attain a level of familiarity and confidence with the controls before teleoperating only through the VR headgear during experiments. During practice runs with the wearable HMI, each user was asked to slowly move their arm leftward, rightward, upward, and downward to confirm if they were able to smoothly manipulate the robotic arm before pick-and-place.

A custom set of 10 post-experiment user survey questions was consolidated into an E-form for the users to express their objective opinions regarding their experience. The survey questionnaire was drafted by taking inspiration from the NASA Task Load Index (NASA-TLX) and System Usability Scale (SUS).

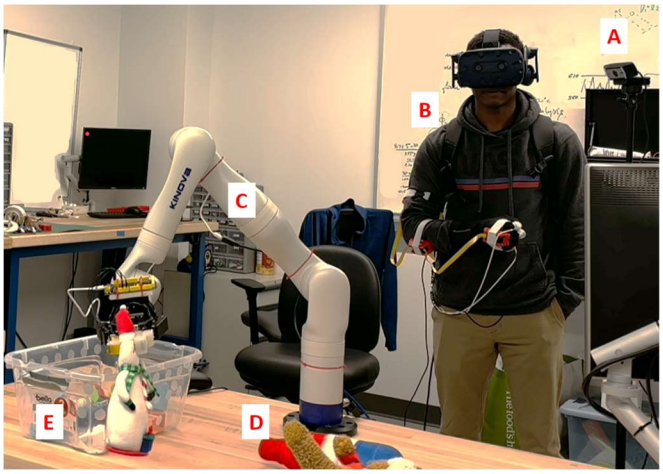

Figure 10. Teleoperation test setup: Camera (A), user wearing the HMI and the VR headgear (B), tele-operated articulated arm (C), target objects (D), and the target object destination (E).

It was found that on an average the users took 95 seconds to achieve the tele-operation objective using the wearable HMI system which was significantly lower than the 138.7 seconds while using the keypad controller as seen in Fig. 11(A). Since the robot mimics the natural movements of the users' arm, the wearable HMI offered more intuitive control than the keypad. The time variant robot gripper force data revealed that, when haptic feedback was made available during the experiment, users took few re-attempts to grasp an object and transfer it to the collection bin within 30 seconds as shown in Fig. 11(B). When haptic feedback was disabled, users found it difficult to perceive the gripper contact with the targeted objects due to the lack of stereoscopic vision that facilitates depth perception. Thus, users made multiple attempts at grasping objects as evident by the random distribution of gripping forces across the duration of the experiment conducted on the set of users (C). It was also observed that the users applied up to 400 g equivalent of gripping force when haptics was enabled and an excessive amount of gripping force of up to 1 kg when haptics was disabled. It was inferred that kinesthetic haptic feedback is effective especially when users do not have visual depth perception due to the absence of stereoscopic vision. Haptics are indispensable for handling fragile objects safely as they have limited structural strength. Further user testing, data acquisition and analysis will be done in the future to explore these new directions.

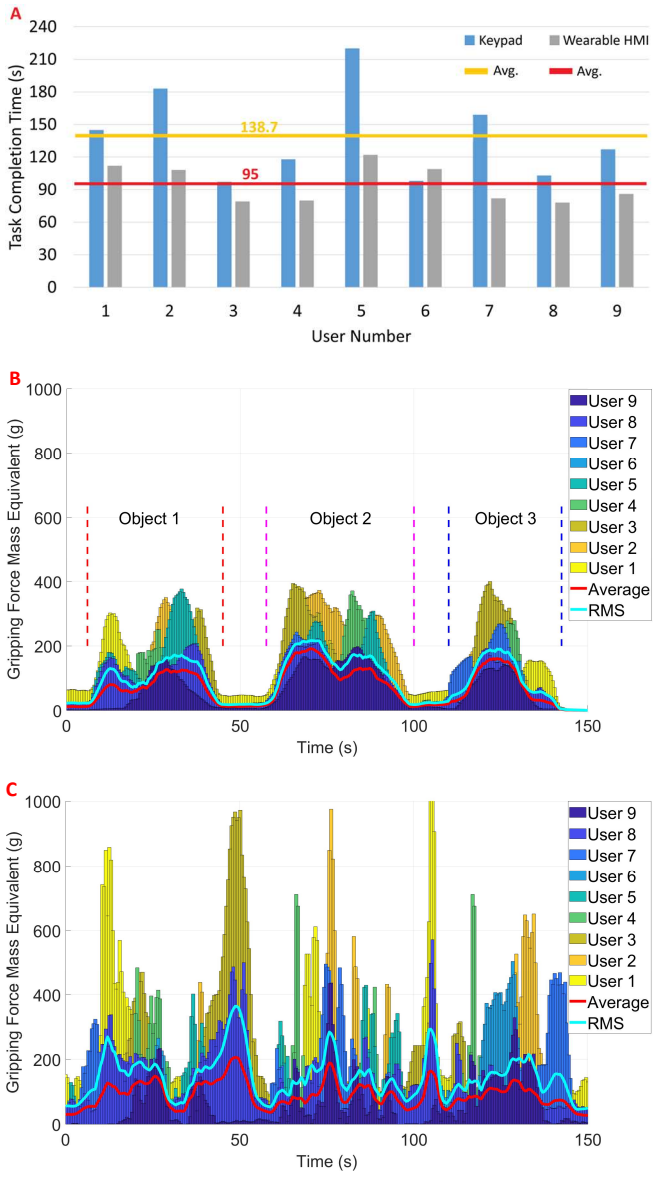

Figure 11. User study data: Task completion time of each participant (A), gripping forces recorded for each user across the experiment while haptics enabled (B), and haptics disabled (C).

V. HMI System Improvements

Based on the experimental studies and surveys conducted, one of the major scopes for improvement in the user

experience is in the wearable HMI's form factor. Instead of separate sensors being strapped individually onto the user, we developed an improved HMI to place all the sensors onto stretchable sleeve and glove units, as shown in Fig. 12, which allow the HMI to be worn comfortably as a normal garment. Owing to its economy, manufacturing scalability and design flexibility, screen printing was used to create both stretchable traces and sensors for the improved HMI [19]. The backpack (labelled A) was interfaced with the sleeve unit through a USB-C connector mounted on a flexible board (B). Four screen-printed stretchable conductive traces (labelled D) were laminated onto the sleeve, of which a pair carried DC power and another pair carried I^2C data for all the sensors. The sleeve was fitted with two IMU modules mounted on flexible boards (C and E) and connected to the four traces for motion capture of the upper and forearm. The sleeve was connected to the glove unit (F) through another USB-C flexible board. The glove unit held a flexible board that carried an IMU module for motion capture of the hand, as well as a Texas Instruments FDC1004 four-channel capacitance-to-digital converter chip that read out the flexion sensors. The flexion sensors consisted of screen-printed stretchable interdigitated capacitors laminated onto the glove thumb and three fingers. The haptic muscles (G) were worn over the glove to provide haptic feedback during teleoperation.

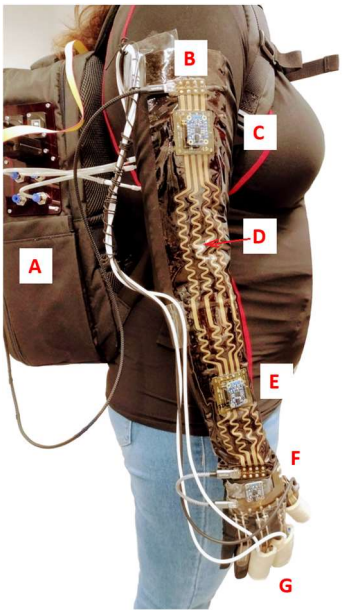

Figure 12. HMI system with stretchable sleeve and glove: HMI backpack (A), USB-C connector (B), upper arm IMU (C), printed stretchable serpentine conductive traces (D), forearm IMU (E), glove unit with hand IMU & printed stretchable flexion sensors for the fingers (F), and haptic muscles (G).

The four stretchable traces (each 2mm in width) consisting of multiple layers of stretchable silver-filled conductor (SE 1109, ACI Materials) were screen-printed onto thermoplastic polyurethane (TPU) stretchable substrates (ESTANE FS H92C4P, Lubrizol) using an MSP-1826PC automated screen printer from HMI. Each layer of conductor was partially cured before printing the next layer. All conductor layers were finally cured in an oven at 140 °C for 5 minutes. The conductors were then encapsulated either by printing a layer of stretchable encapsulant (SE 3104, ACI Materials) followed by curing in an oven at 140 °C for 10 minutes, or by laminating a softer TPU substrate (ESTANE FSL75A4P, Lubrizol) at 120 °C for 15 minutes. To ensure smooth data and power transmission along the ~50cm-long traces running the length of the sleeve, a target was set that the resistance of the stretchable conductors should not exceed 100 Ω [20] even after cyclic stretch-testing at 40% strain (from 0% to 40% and back to 0% strain during each cycle) for 1,000 cycles at 15 cycles/min, which is considered to be more severe stretching than the sleeve will experience during HMI use. This target was more than satisfied by printing four layers of the stretchable silver conductor in a serpentine pattern having 2mm arc radius, for which the average initial resistance was 2.8Ω and the average final resistance was 25.8Ω after cyclic stretch-testing. The encapsulated conductive traces were then laminated onto the stretchable spandex fabric of the sleeve using TPU hot-melt film (ESTANE FS HM70A71, Lubrizol). The same materials and manufacturing approach were used for screen-printing, encapsulating and laminating the interdigitated capacitive finger flexion sensors onto the glove fingers, except that only one layer of conductor was needed and the sensors were printed on the softer TPU substrate. The flexible boards carrying USB-C connectors, IMU modules, and capacitance measurement chips were electrically connected to the printed stretchable conductors and sensors using stretchable conductive adhesive (TS 1334, ACI Materials), while TPU hot-melt was used to make a robust mechanical connection. The adhesive was cured in the oven at 140 °C for 60 minutes.

In-plane interdigitated capacitive strain sensors were chosen for tracking finger flexion because they can stretch to larger strains with better recovery and smaller drift compared to resistive sensors. An interdigitated sensor design of fingers with 200 µm width and 150 µm spacing was chosen. This design yielded an acceptable average sensitivity of 0.4% change in capacitance per % change in strain, while showing a very low drift of 1.1 % change in capacitance after 1,000 cycles of cyclic stretch-testing from 0 to 40% strain as seen in Fig. 13(A). The sensors were laminated onto the knuckles of the glove fingers (C, D, E), and were read out individually. When the fingers are flexed the sensors are stretched, and the capacitance decreased, thus enabling the motion tracking. Since the pneumatic haptic muscles are worn on the fingers, over the finger flexion sensors, there is possibility of cross-talk between the haptic muscles and the sensors. The response of the sensor to full finger flexion, half finger flexion, and inflation of the overlying pneumatic haptic muscle to different pressures from 0 to 6 psi is shown in Fig. 13(F). The sensor's capacitance (~14 pF initially) decreased by ~8 pF when the finger was fully flexed, showing that the sensitivity was highly sufficient for tracking the finger flexion. The sensor continued to perform properly when the overlying pneumatic haptic muscle was inflated, and the capacitance increased by ~ 2 pF when the muscle was fully inflated to 6 psi. The response of the sensor to the pressure was quite linear, therefore it was likely that any cross-talk between the haptic muscle and the sensor could be corrected in the system software. After having tested the individual capacitive sensors, it was integrated with the capacitance read-out chip board to make the motion capture glove unit. The whole flexible motion capture system was connected to the HMI backpack and was successfully utilized for tele-operating the articulated robotic arm to perform a pick and place task (see supplementary video).

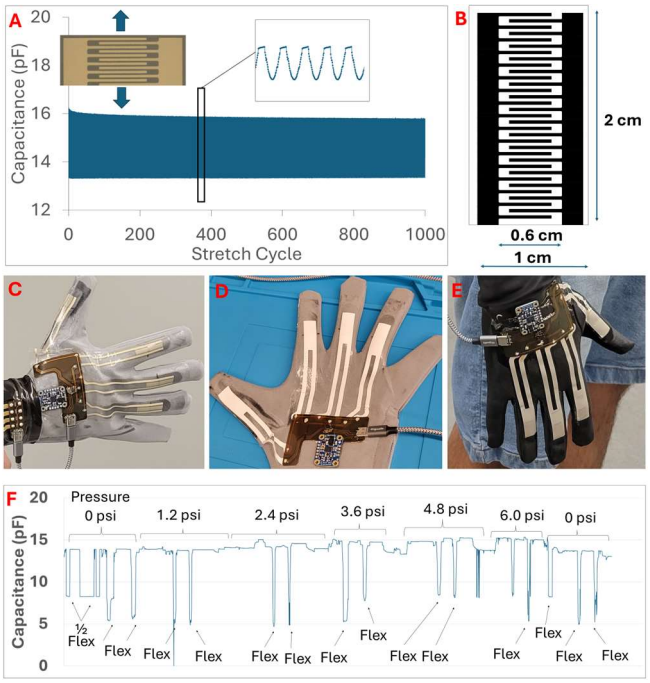

Figure 13. Electromechanical (stretching) performance of the interdigitated capacitive flexion sensor (A) in which the direction of stretch is shown with arrows in the inset image. Dimensions of the sensor (B). Capacitive sensor on glove with soft TPU encapsulation (C). Capacitive sensor on glove with printed encapsulation (D & E). Response of sensor when the finger is flexed and when the overlying haptic muscle is pressurized (F).

VI. Conclusion And Future Work

We successfully engineered a tetherless soft robotic wearable HMI system and validated its functionality in teleoperating a Kinova Gen 3 articulated robotic arm while viewed via a VR headgear. We developed a woven fabric based elastomeric pneumatic muscles to render haptic feedback. We presented a comparative analysis of the pressure and force transfer characteristics of this muscle (DOWSIL) and the muscle developed by our group in a previous work (EcoFlex 0030). We found that both the muscles show linear pressure response to the PWM input beyond the dead zone of 10% in case of DOWSIL and 15% in case of EcoFlex 0030. It was observed that the EcoFlex30 variant showed wider linear operating range and higher restoration force than DOWSIL. We also developed a 3D Hall effect force sensor to measure the grasp force at the robot's end-effector. We conducted a pilot user study to validate the efficacy of the HMI system. It was observed that the average time taken by the users to perform the teleoperation task with the HMI was 31.4% less than the keypad controller. When haptics was enabled, users applied 60% less gripping force compared to when it was disabled. A stretchable sleeve and glove unit was developed to enhance the form factor of the HMI system and was successfully interfaced with it.

The future aim is to improve the reliability of the interconnections that connect the flex boards and sensors to the stretchable traces. Also, mitigation of the proximity issues encountered by capacitive sensors when brought near other objects. We plan to conduct more extensive user studies to validate the performance and reliability of the glove and sleeve unit for teleoperation.

References

[1] B. Ma, Z. Jiang, Y. Liu, and Z. Xie, "Advances in Space Robots for On-Orbit Servicing: A Comprehensive Review", *Adv. Intell. Syst*., Apr.2023, Vol.5, Issue 8, 2200397.

[2] E. Ackerman, "How Diligent's Robots Are Making a Difference in Texas Hospitals", *IEEE Spectrum*, Mar.2020.

[3] T. Gao, J. Yan, X. Yang, C. Hua and X. Guan, "Teleoperation System of Autonomous Underwater Vehicle Toward Human-on-the-Loop: Design and Implementation", *2023 IEEE 13th International Conference on CYBER Technology in Automation, Control, and Intelligent Systems (CYBER)*, Qinhuangdao, China, 2023, pp. 142-147.

[4] A. C. Chen, M. Hadi, P. Kazanzides and E. Azimi, "Mixed Reality Based Teleoperation of Surgical Robotics", *2023 International Symposium on Medical Robotics (ISMR)*, 2023, pp. 1-7.

[5] M.D. Moniruzzaman, A. Rassau, D. Chai, S.M.S. Islam, "Teleoperation methods and enhancement techniques for mobile robots: A comprehensive survey", *Robotics and Autonomous Systems*, Apr. 2022, vol.150, 103973, ISSN 0921-8890.

[6] R. V. Patel, S. F. Atashzar and M. Tavakoli, "Haptic Feedback and Force-Based Teleoperation in Surgical Robotics", *Proceedings of the IEEE*, vol. 110, no. 7, pp. 1012-1027, July 2022.

[7] Y. Huang, K. Yao, J. Li, D. Li, H. Jia, Y. Liu, C. K. Yiu, W. Park and X. Yu, "Recent advances in multi-mode haptic feedback technologies towards wearable interfaces", *Materials Today Physics*, Jan. 2022, vol. 22, 100602, ISSN 2542-5293.

[8] Z. Sun, M. Zhu, X. Shan and C. Lee, "Augmented tactile-perception and haptic-feedback rings as human-machine interfaces aiming for immersive interactions", *Nat Commun*, Sept. 2022, vol.13, 5224.

[9] S. H. Ko and J. Rogers., "Functional Materials and Devices for XR(VR/AR/MR) Applications", *Adv. Func. Materials,* Sept. 2021, vol. 31, 2106546.

[10] M. Fleury, G. Lioi, C. Barillot and A. Lécuyer, "A Survey on the use of Haptic Feedback for Brain -Computer Interfaces and Neuro feedback", *Front Neurosci*., Jun. 2020, vol.14, 528.

[11] R. Rameshwar, E. H. Skorina and C. D. Onal, "Fabric-Silicone Composite Haptic Muscles for sensitive Wearable Force Feedback", PETRA'2023*: Proceedings of the 16th International Conference on Pervasive Technologies to Assistive Environments,* July 2023.

[12] A. Dwivedi, A. Ramakrishnan, A. Reddy, K. Patel, S. Ozel and C. D. Onal, "Design, Modeling, and Validation of a Soft Magnetic 3-D Force Sensor", in *IEEE Sensors Journal*, May 2018, vol. 18, pp. 3852-63.

[13] A. M. Votta, S. Y. Günay, D. Erdogmus and C. Onal, "Force-Sensitive Prosthetic Hand with 3- axis Magnetic Force Sensors", *IEEE International Conference on Cyborg and Bionic Systems (CBS)*, Munich, Germany, 2019, pp. 104-109.

[14] Soft Robotics Toolkit, "StretchSense" (accessed Feb. 25, 2024) https://softroboticstoolkit.com/stretchsense.

[15] J. Qin, L.-J. Yin, Y.-N. Hao, S.-L. Zhong, D.-L. Zhang, K. Bi, Y.-X. Zhang, Y. Zhao, Z.-M. Dang, "Flexible and Stretchable Capacitive Sensors with Different Microstructures", *Adv. Mater*., 2021, vol. 33, 2008267.

[16] Zhuyu Ma, Yang Zhang, Kaiyi Zhang, Hua Deng, Qiang Fu, "Recent progress in flexible capacitive sensors: Structures and properties", *Nano Materials Science*, Spt. 2023, vol. 5, Issue 3, pp. 265-277.

[17] A. Edeer, Z. Tulum, L. Pinar, and F. Başkurt, "Comparison of Pressure Pain Threshold, Grip Strength, Dexterity and Touch Pressure of Dominant and Non-Dominant Hands within and Between Right- and Left-Handed Subjects", *Journal of Korean medical science*, Jan. 2005, vol.19, pp.874–878.

[18] A. J. Doxon, D. E. Johnson, H. Z. Tan and W. R. Provancher, "Human Detection and Discrimination of Tactile Repeatability, Mechanical Backlash, and Temporal Delay in a Combined Tactile-Kinesthetic Haptic Display System", in *IEEE Transactions on Haptics*, Oct.-Dec. 2013, vol. 6, no. 4, pp. 453-463.

[19] M. U. Ahmed, M. M. Hossain, M. Safavieh, Y. L. Wong, I. A. Rahman, M. Zourob and E. Tamiya, "Toward the development of smart and low cost point-of-care biosensors based on screen printed electrodes", *Crit.Rev. Biotechnol*., Jan. 2015, vol.36, pp. 495-505.

[20] NXP Semiconductors, "Sending I^2C-bus signals via long communications cables", *Application Note AN10658,* Feb. 2008.